Available online at www.sciencedirect.com
ScienceDirect
Trans. Nonferrous Met. Soc. China 35(2025) 3020−3029
Transactions of Nonferrous Metals Society of China
www.tnmsc.cn

Influence of W-doping on microstructure, mechanical and thermal properties of TiAlSiN coatings

Xu SUN[1], Wen HU[2], Li CHEN[1,2], Jian-chuan WANG[1]

1. State Key Laboratory of Powder Metallurgy, Central South University, Changsha 410083, China;
2. Zhuzhou Cemented Carbide Cutting Tools Co., Ltd., Zhuzhou 412007, China

Received 18 January 2024; accepted 19 April 2024

Abstract: The effect of W-doping on the structure and properties of TiAlSiN coatings was investigated through scanning electron microscopy, X-ray diffraction, differential scanning calorimetry, and nanoindentation. Tungsten doping in the coatings forms both substitution solid solution of Ti and/or Al in TiAlN and W simple substance. W-addition improves the surface quality of the coatings. $Ti_{0.46}Al_{0.45}Si_{0.09}N$, $Ti_{0.43}Al_{0.46}Si_{0.08}W_{0.03}N$, and $Ti_{0.41}Al_{0.46}Si_{0.07}W_{0.06}N$ present similar hardness of (29.1±0.4), (29.7±1.1), and (30.2±1.0) GPa, respectively. During annealing, $Ti_{0.41}Al_{0.46}Si_{0.07}W_{0.06}N$ achieves peak hardness of (35.3±1.0) GPa at 1100 °C, whereas those of $Ti_{0.46}Al_{0.45}Si_{0.09}N$ and $Ti_{0.43}Al_{0.46}Si_{0.08}W_{0.03}N$ are only (33.1±0.8) and (33.9±0.8) GPa at 1000 °C. Furthermore, moderate W-addition (3 at.%) upgrades the oxidation resistance of TiAlSiN. After oxidation at 1000 °C for 10 h, the oxide thicknesses of $Ti_{0.46}Al_{0.45}Si_{0.09}N$, $Ti_{0.43}Al_{0.46}Si_{0.08}W_{0.03}N$, and $Ti_{0.41}Al_{0.46}Si_{0.07}W_{0.06}N$ are ~0.70, ~0.52, and ~0.90 μm, respectively.
Key words: TiAlSiWN coating; cathodic arc evaporation; structural evolution; hardness; thermal stability; oxidation resistance

1 Introduction

Concern about the working accuracy and service life of cutting tools under harsh and complex conditions has become a core problem in modern industry, and as a result considerable research has focused on the transition metal nitrides (TMN) coatings prepared by physical vapor deposition (PVD) that can effectively protect the cutting tools [1−3]. Among them, TiAlSiN coatings are extensively employed in the machine manufacturing field, directly linked to their high hardness, excellent thermal stability, age-hardening effect triggered by spinodal decomposition, and outstanding oxidation resistance [4,5]. Si-existence within the TiAlSiN coatings is either substitution solid solution of Si in TiAlN or/and nanoscale TiAlN crystallites surrounded by amorphous (a-) SiN_x, which is related to the Si content and deposition parameters [6−8]. YU et al [7] found that a small amount of Si-addition results in the Si solid solution and thereby brings about a slight increment in hardness originating from the solid-solution strengthening as well as fine-grained strengthening, while the formation of nanocomposite with increasing Si content in the range of (4−10) at.% allows for a significantly increased hardness. Compared with TiAlN coatings, the TiAlSiN coatings reveal a remarkable oxidation resistance due to the delayed anatase-to-rutile TiO_2 transformation and the earlier generation of dense Al-rich oxide top-layer [9]. Recently, related studies have claimed that the oxidation resistance benefits

Corresponding author: Li CHEN, Tel: +86-13975870633, E-mail: chenli_927@126.com;
Jian-chuan WANG, Tel: +86-13080566873, E-mail: jcw728@126.com
https://doi.org/10.1016/S1003-6326(25)66863-4

from the SiO_2 generation, which allows to "seal" the grain boundaries, pores, and the interfaces of the oxide scale to the remaining nitride [10,11]. However, alloying with Si decreases the metastable solution limit of AlN in c-TiN and promotes the wurtzite (w-) AlN formation, which has an adverse effect on the mechanical properties [12].

Currently, some investigations utilize multiple alloying methods to stabilize the cubic growth of $Ti_{1-x-y}Al_xSi_yN$ coatings and further enhance their comprehensive performance. Incorporation of Ta facilitates the cubic growth of TiAlSiN coatings by enlarging the metastable solubility limitation of AlN in c-TiN, and thereby leads to an improvement in their mechanical and thermal properties [13]. Ag-addition into TiAlSiN coatings, which modifies the outermost protective oxide layer to delay the oxidation failure, has a positive effect on the oxidation resistance [14]. ASANUMA et al [15] proposed that incorporation of Ce significantly improves the thermal stability and oxidation resistance of TiAlSiN coatings.

Except for the alloying elements listed above, tungsten (W), which can optimize the toughness and friction performance of nitride coatings, has been published in a large number of literatures [16−18]. Alloying with W into TiN coatings induces a simultaneous hardening and toughening effects, arising from the variation of the bonding character [19]. GLATZ et al [20] indicated that incorporating up to 10 at.% W into TiAlN delays the w-AlN formation during annealing. Furthermore, a special Guinier−Preston (GP) zone hardening in W-containing coatings with a low Al/(Al+Ti) atomic ratio was reported by PSHYK et al [21], benefiting from the generation of atomic-layer-thick ordered W planes. This structure coherent with the cubic matrix is introduced by the atomic arrangement in annealing, which strongly obstructs the dislocation motion and leads to a continuous increase in the hardness of $Ti_{0.53}Al_{0.39}W_{0.08}N$ coating even though the soft w-AlN phase has already appeared. Moreover, the W-addition improves the melting point of the target, and thereby reduces the droplet defects induced by the arc evaporation, which upgrades the surface quality and coating homogeneity [20,22].

As mentioned above, W-doping is widely used to tailor the surface quality and comprehensive performance of coatings, whereas there is little research about the effect of W-doping on the structure and properties of the TiAlSiN coatings. In this work, the influence of W-doping on the microstructure, mechanical and thermal properties of the TiAlSiN coating was investigated, which could provide a promising candidate for protective coatings in the machine manufacturing field.

2 Experimental

TiAlSiN and TiAlSiWN coatings were prepared with $Ti_{0.40}Al_{0.50}Si_{0.10}$, $Ti_{0.38}Al_{0.50}Si_{0.10}W_{0.02}$, and $Ti_{0.36}Al_{0.50}Si_{0.10}W_{0.04}$ targets (99.99% purity) using a commercial cathodic arc evaporation deposition system (Oerlikon Balzers INNOVA). To minimize the possible residual contamination, various substrates including low-alloy steel foils (200 mm × 200 mm × 0.05 mm), cemented carbide (WC−6wt.%Co, 5 mm × 5 mm × 20 mm), W plates (11 mm × 11 mm × 2 mm), and polycrystalline Al_2O_3 sheets (25 mm × 5 mm × 0.05 mm), employed for structure and properties measurements, were subjected to 20 min Ar ion etching under 0.3 Pa Ar pressure and −170 V substrate bias. The vacuum chamber, which was sealed well and not affected by the ambient atmosphere, was pumped down to 1.0×10^{-3} Pa and heated to 500 °C prior to deposition. The deposition parameters are as follows: 3.2 Pa N_2 pressure, 500 °C deposition temperature, −40 V substrate bias, and 180 A target current.

To obtain the free-standing coating powder, the coated low-alloy steel was immersed into 10 mol.% nitric acid followed by grinding. Subsequently, annealing of powder specimens was conducted by STA 409C differential scanning calorimetry (DSC) instrument (Netzsch, Germany) in Ar (99.9% purity) and synthetic air (79 vol.% N_2, 21 vol.% O_2, 20 mL/min flowing rate) atmosphere at target temperatures with heating and cooling rates of 10 and 50 K/min. Coated Al_2O_3 sheets were isothermally oxidized at 1000 °C for 10 h in the synthetic air with the same heating and cooling rates using the DSC instrument. In addition, W-coated plates were annealed in a vacuum furnace (COD533R, pressure $<1\times10^{-3}$ Pa) for 30 min at specified temperatures (T_a=800−1200 °C in steps of 100 °C) with a heating rate of 10 K/min, followed by natural cooling to room temperature (RT).

Surface and cross-sectional morphologies of

as-deposited and oxidized coatings were observed by scanning electron microscopy (SEM, Zeiss Supra55), and the attached energy dispersive X-ray spectroscopy (EDX, Oxford Instrument X-Max) was used to test the composition and elemental distribution. Phase structures of coatings in as-deposited, annealed, and oxidized states were investigated by X-ray diffraction (XRD, Bruker AXS D8 Advance) with Cu K_α radiation. In light of the Oliver and Pharr method [23], hardness and elastic modulus of as-deposited and annealed coatings on W plates were measured more than 15 times under a penetration load of 15 mN and a holding time of 15 s using Anton Paar NHT^2 nanoindentation equipped with a Berkovich diamond tip. The relatively low load was chosen to ensure that the indentation depth is less than 10% of the coating thickness, which avoids the influence of the substrate on the accuracy of the experiments.

3 Result and discussion

3.1 Microstructure and mechanical properties

The chemical compositions of coatings by EDX are $Ti_{0.46}Al_{0.45}Si_{0.09}N$, $Ti_{0.43}Al_{0.46}Si_{0.08}W_{0.03}N$, and $Ti_{0.41}Al_{0.46}Si_{0.07}W_{0.06}N$, respectively, corresponding to $Ti_{0.40}Al_{0.50}Si_{0.10}$, $Ti_{0.38}Al_{0.50}Si_{0.10}W_{0.02}$, and $Ti_{0.36}Al_{0.50}Si_{0.10}W_{0.04}$ targets. The (Ti+Al+Si+W)/N atomic ratios are normalized to 1 for easier reading. A slight decline in the amount of light Al and Si elements compared to that of corresponding targets arises from their greater susceptibility to gas scattering and re-sputtering effects as well as lower ionization rates during deposition [24].

Figure 1 shows the XRD patterns of as-deposited coatings. A mixed cubic and wurtzite structure of $Ti_{0.46}Al_{0.45}Si_{0.09}N$ coating is observed. Our previous research indicated that Si-existence is both substitution solid solution of Ti and/or Al in TiAlN and amorphous SiN_x accumulating at the grain boundaries [25]. The $Ti_{0.43}Al_{0.46}Si_{0.08}W_{0.03}N$ and $Ti_{0.41}Al_{0.46}Si_{0.07}W_{0.06}N$ coatings exhibit a three-phase structure of c/w-(Ti, Al, Si, W)N and bcc-W. In agreement with the previous TEM investigations of the TiSiWN coatings [22], both W-solution and W simple substance appear within coatings. Additionally, the intensity of w-AlN diffraction peaks decreases with elevated W-content. This means that incorporation of W into TiAlSiN increases the solid solution limitation of Al in TiN.

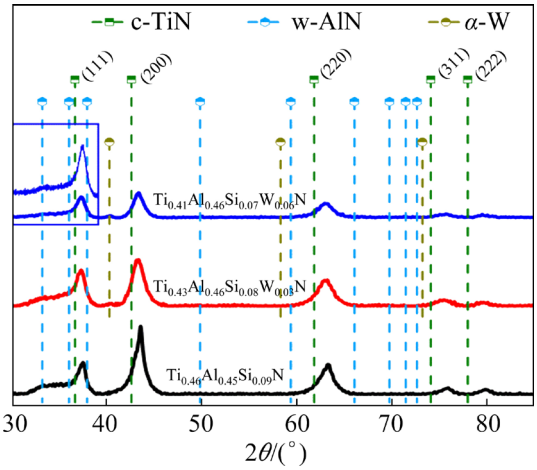

Fig. 1 XRD patterns of as-deposited $Ti_{0.46}Al_{0.45}Si_{0.09}N$, $Ti_{0.43}Al_{0.46}Si_{0.08}W_{0.03}N$, and $Ti_{0.41}Al_{0.46}Si_{0.07}W_{0.06}N$ coatings

Figure 2 shows the surface and cross-sectional fracture SEM images of $Ti_{0.46}Al_{0.45}Si_{0.09}N$, $Ti_{0.43}Al_{0.46}Si_{0.08}W_{0.03}N$, and $Ti_{0.41}Al_{0.46}Si_{0.07}W_{0.06}N$ coatings. A large number of growth defects including macro-particles and holes can be observed on the surface of the $Ti_{0.46}Al_{0.45}Si_{0.09}N$ coating (see Fig. 2(a)). Alloying with W leads to a drop in the size and quantity of the growth defects (see Figs. 2(b, c)). A significant improvement in the surface quality is observed by the $Ti_{0.41}Al_{0.46}Si_{0.07}W_{0.06}N$ coating.

The process of preparing coatings by cathodic arc evaporation equipment usually accompanies the inhomogeneous evaporation behavior of the target material, where part of the unionized macro-particles move towards the substrates with the ionized metal vapors. However, these macro-particles exhibit low adhesive strength to the coating and are prone to spalling under a high stress level, resulting in a large number of holes on the surface of coatings. In general, the state of macro-particles is closely related to the melting point of the target material [26,27]. For the W-containing coatings, the incorporation of W with high melting point is helpful to reduce the melting zones of the target during evaporation, which avoids the pile-up effect on the target surface. In this case, the ejection of huge macro-particles is effectively diminished, thereby smoothing the surface of coatings. This phenomenon was also found by GLATZ et al [20].

In addition, as shown in Figs. 2(d−f), the thicknesses of $Ti_{0.46}Al_{0.45}Si_{0.09}N$ (~3.03 μm),

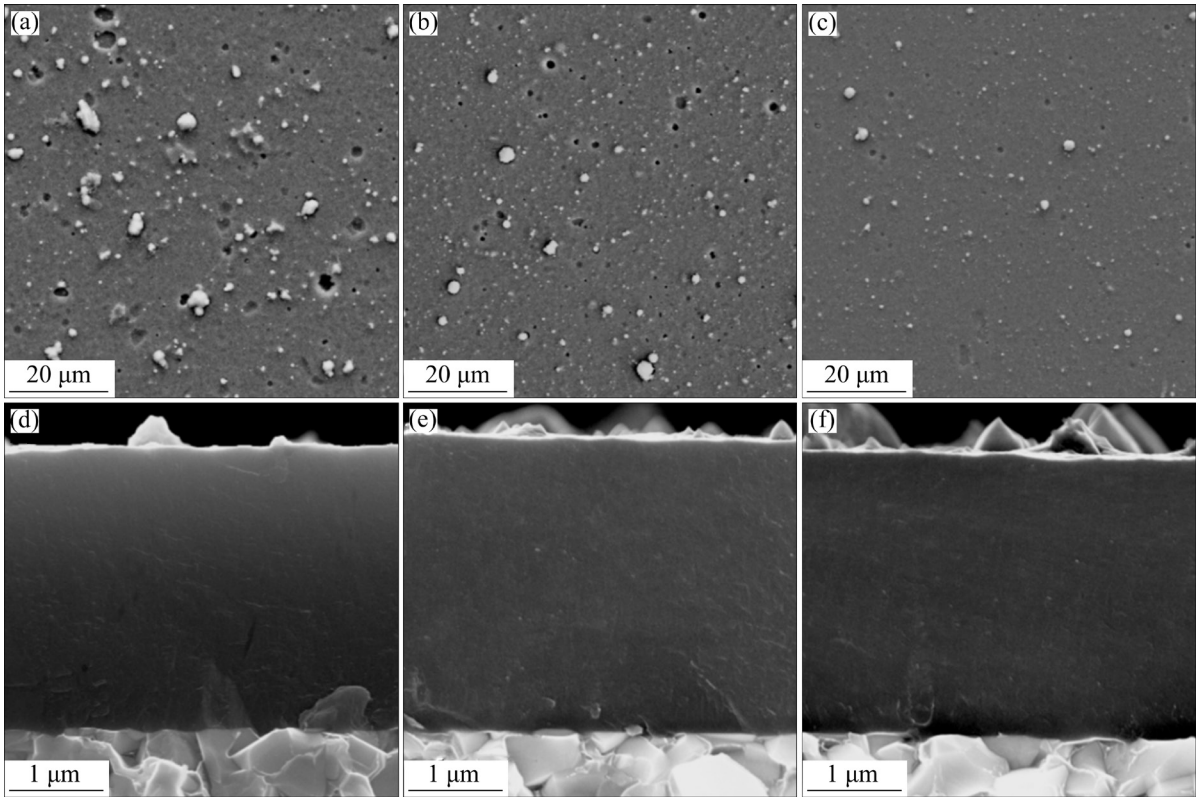

Fig. 2 Surface (a−c) and fracture (d−f) SEM images of as-deposited coatings: (a, d) $Ti_{0.46}Al_{0.45}Si_{0.09}N$; (b, e) $Ti_{0.43}Al_{0.46}Si_{0.08}W_{0.03}N$; (c, f) $Ti_{0.41}Al_{0.46}Si_{0.07}W_{0.06}N$

$Ti_{0.43}Al_{0.46}Si_{0.08}W_{0.03}N$ (~3.14 μm), and $Ti_{0.41}Al_{0.46}Si_{0.07}W_{0.06}N$ (~2.98 μm) are essentially the same. The competitive growth of cubic and wurtzite phases strongly limits grain boundary migration, leading to fine crystalline grains [28]. Therefore, all coatings present a smooth fracture and featureless growth structure.

The hardness and elastic modulus of as-deposited coatings are depicted in Fig. 3. Generally, the solid solution hardening of Si-substitution and the resistant dislocation movement of the a-SiN_x interfacial phase induce a high hardness for Si-containing coatings [29]. However, the hardness of the $Ti_{0.46}Al_{0.45}Si_{0.09}N$ coating is only (29.1±0.4) GPa, due to the large fraction of soft w-AlN-based phase [30]. Alloying with W has no obvious enhancement effect on the hardness of (29.7±1.1) GPa for $Ti_{0.43}Al_{0.46}Si_{0.08}W_{0.03}N$ and (30.2±1.0) GPa for $Ti_{0.41}Al_{0.46}Si_{0.07}W_{0.06}N$. This is in good consistent with Ref. [22], where the W-addition brings about the precipitation of the bcc-W phase, and thereby the weakening effect of the comparatively soft W simple substance overcompensates the solid solution hardening of the

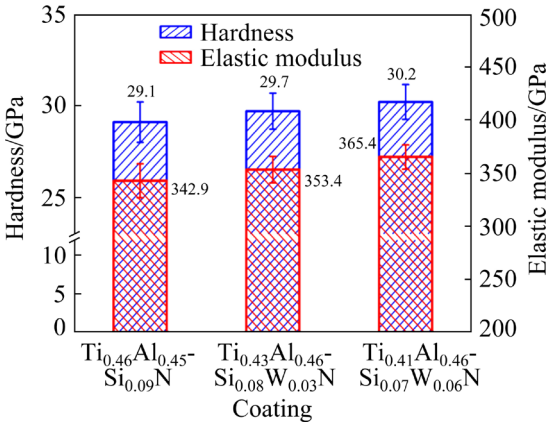

Fig. 3 Hardness and elastic modulus of as-deposited $Ti_{0.46}Al_{0.45}Si_{0.09}N$, $Ti_{0.43}Al_{0.46}Si_{0.08}W_{0.03}N$, and $Ti_{0.41}Al_{0.46}Si_{0.07}W_{0.06}N$ coatings

W-addition as well as the fine grain strengthening of the Si-addition [20,31]. Moreover, a drop in the fraction of w-AlN-based phase with the W-addition gives rise to a continuous increase in elastic modulus from (342.9±16.0) GPa for $Ti_{0.46}Al_{0.45}Si_{0.09}N$ to (353.4±12.4) GPa for $Ti_{0.43}Al_{0.46}Si_{0.08}W_{0.03}N$, and to (365.4±11.4) GPa for $Ti_{0.41}Al_{0.46}Si_{0.07}W_{0.06}N$.

3.2 Thermal stability

Figure 4 displays the phase evolution of $Ti_{0.46}Al_{0.45}Si_{0.09}N$, $Ti_{0.43}Al_{0.46}Si_{0.08}W_{0.03}N$, and $Ti_{0.41}Al_{0.46}Si_{0.07}W_{0.06}N$ coatings during annealing. As shown in Fig. 4(a), the diffraction peaks of the $Ti_{0.46}Al_{0.45}Si_{0.09}N$ coating have no visible change at T_a of 800−900 °C, except for a gentle shift to a high 2θ angle triggered by the recovery process [32,33]. Upon annealing to 1000 °C, the broadening of the cubic (111) and (200) peaks signifies the occurrence of spinodal decomposition [34]. Besides, there is also a slight increase in the intensity of w-AlN peaks owing to the decomposition of the wurtzite phase matrix. As the T_a rises to 1450 °C, the $Ti_{0.46}Al_{0.45}Si_{0.09}N$ coating has been fully decomposed into the stable c-TiN and w-AlN phases.

W-containing coatings behave a similar thermal decomposition process with $Ti_{0.46}Al_{0.45}Si_{0.09}N$ (see Figs. 4(b, c)). Only the intensity of XRD peaks for the w-AlN-based phase is low during annealing. Especially, after annealing at 1200 and 1300 °C, increasing W content leads to a continuous drop in the intensity of XRD peaks for the w-AlN-based phase. This hints that the W-addition retards the thermal decomposition of the TiAlSiN coating, in good agreement with the researches in Refs. [20,35]. Besides, the fraction of the bcc-W phase also exhibits a growing trend with increasing annealing temperature. After annealing at 1450 °C, the W-containing coatings fully decompose into c-TiN, w-AlN, bcc-W, W_5Si_3, and Si_2W phases.

Figure 5 shows the hardness variation of the coatings as a function of annealing temperature. The $Ti_{0.46}Al_{0.45}Si_{0.09}N$ coating with mixed cubic and wurtzite structure reaches a peak hardness of (33.1±0.8) GPa after annealing at 1000 °C. This can be attributed to the age-hardening effect stemming from the spinodal decomposition. The coherent strain between the cubic matrix and nanoscale Al-rich as well as Ti-rich domains plays an essential role. In addition, as for the wurtzite Ti−Al−N coatings, SALAMANIA et al [36] pointed out that the forming nanoprecipitates during annealing have a semicoherent relationship with the surrounding wurtzite matrix, which also assists in the impeding glide and motion of dislocation, and thereby results in the hardness increment. Further temperature increase results in a distinct decline in hardness due to the coarsening of the spinodal decomposition products and the formation of soft w-AlN, where the hardness decreases to (32.9±0.9) GPa at 1100 °C and (29.5±1.0) GPa at 1200 °C.

In comparison, increasing W content allows for better high-temperature mechanical properties in annealing. The $Ti_{0.43}Al_{0.46}Si_{0.08}W_{0.03}N$ and $Ti_{0.41}Al_{0.46}Si_{0.07}W_{0.06}N$ coatings attain their maximum hardness of (33.9±0.8) GPa at 1000 °C and (35.3±1.0) GPa at 1100 °C, respectively. Except for the age-hardening effect as well as retarded w-AlN formation discussed in Fig. 4, the Guinier−Preston zones formed by atomic-plane-thick W disks populating {111} planes in the coatings hinder the movement of dislocation, thereby contributing to

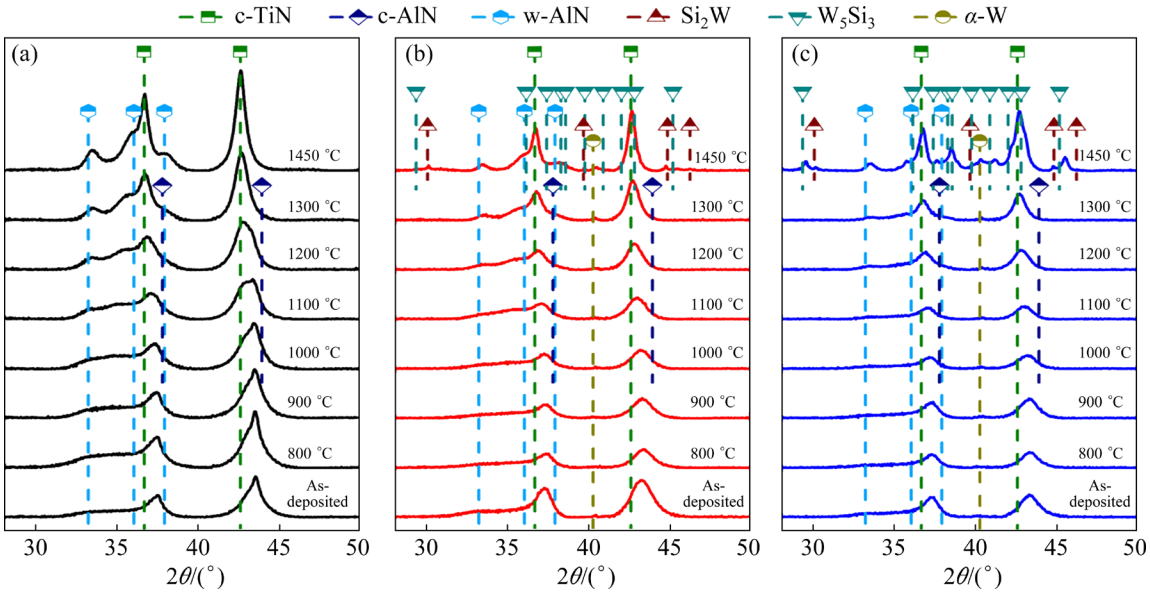

Fig. 4 XRD patterns of $Ti_{0.46}Al_{0.45}Si_{0.09}N$ (a), $Ti_{0.43}Al_{0.46}Si_{0.08}W_{0.03}N$ (b), and $Ti_{0.41}Al_{0.46}Si_{0.07}W_{0.06}N$ (c) coatings after annealing at different temperatures

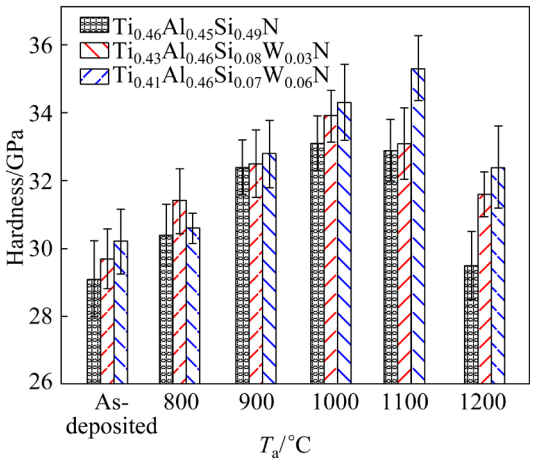

Fig. 5 Hardness of $Ti_{0.46}Al_{0.45}Si_{0.09}N$, $Ti_{0.43}Al_{0.46}Si_{0.08}W_{0.03}N$, and $Ti_{0.41}Al_{0.46}Si_{0.07}W_{0.06}N$ coatings as function of annealing temperature

the hardness enhancement of W-containing coatings during annealing [21]. Furthermore, the coherent nanoscale domains of the Guinier-Preston zone and cubic matrix, which induce coherency strains and Koehler-type hardening [37,38] due to the difference in elastic shear modulus of the modulation layers, can also counteract the effect of softer w-AlN. After annealing at 1200 °C, as a consequence of the grain coarsening and the increasing phase fractions of soft bcc-W as well as the w-AlN formation, the hardness finally decreases to (31.6±0.7) GPa for $Ti_{0.43}Al_{0.46}Si_{0.08}W_{0.03}N$ and (32.4±1.2) GPa for $Ti_{0.41}Al_{0.46}Si_{0.07}W_{0.06}N$, which are still higher than those of the as-deposited states.

3.3 Oxidation resistance

To investigate the oxidation mechanism of W-doped TiAlSiN coatings, XRD analyses of the powdered $Ti_{0.46}Al_{0.45}Si_{0.09}N$, $Ti_{0.43}Al_{0.46}Si_{0.08}W_{0.03}N$, and $Ti_{0.41}Al_{0.46}Si_{0.07}W_{0.06}N$ coatings are performed at specified temperatures (800−1200 °C) in synthetic air. As depicted in Fig. 6(a), the oxidation of $Ti_{0.46}Al_{0.45}Si_{0.09}N$ occurs at 900 °C with the appearance of a- and r-TiO_2 peaks, followed by the formation of the α-Al_2O_3 phase as well as the intensified transformation from anatase to rutile at T_{ox}=1000 °C [39]. After oxidation at 1100 °C, the diffraction peaks of nitride disappear, suggesting the total oxidation of $Ti_{0.46}Al_{0.45}Si_{0.09}N$. Notably, the diffraction peaks of a-TiO_2 can still be detected at T_{ox}=1200 °C since Si-addition postpones the anatase-to-rutile TiO_2 transformation [9].

The onset temperature of oxidation for $Ti_{0.43}Al_{0.46}Si_{0.08}W_{0.03}N$ decreases to 800 °C with the appearance of tiny a- and r-TiO_2 diffraction peaks (see Fig. 6(b)). Also the intensity of α-Al_2O_3 diffraction peaks for $Ti_{0.43}Al_{0.46}Si_{0.08}W_{0.03}N$ at 1000 °C is stronger than that of W-free $Ti_{0.46}Al_{0.45}Si_{0.09}N$. In general, more protective α-Al_2O_3 formation is profitable for the oxidation resistance [10,40]. Therefore, the terminal oxidation temperature of the $Ti_{0.43}Al_{0.46}Si_{0.08}W_{0.03}N$ is delayed to 1200 °C, and the oxide products consist of r-TiO_2, α-Al_2O_3, and $Al_6Si_2O_{13}$ phases. Among them, the new oxide $Al_6Si_2O_{13}$ is formed by the sintering of SiO_2 and α-Al_2O_3. However, the higher W content

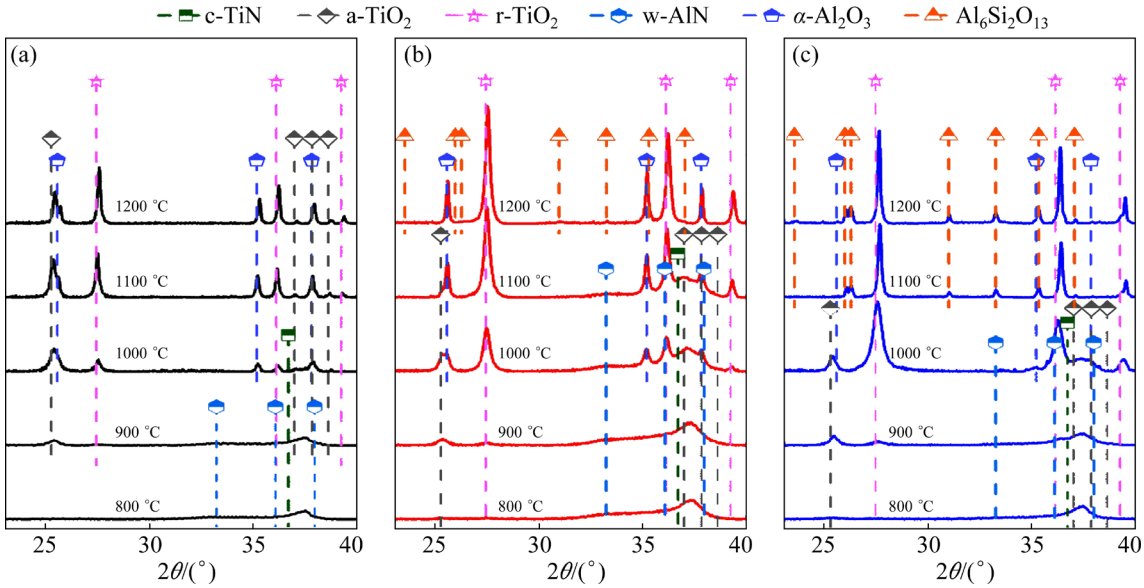

Fig. 6 XRD patterns of $Ti_{0.46}Al_{0.45}Si_{0.09}N$ (a), $Ti_{0.43}Al_{0.46}Si_{0.08}W_{0.03}N$ (b), and $Ti_{0.41}Al_{0.46}Si_{0.07}W_{0.06}N$ (c) coatings after oxidation in synthetic air at different temperatures

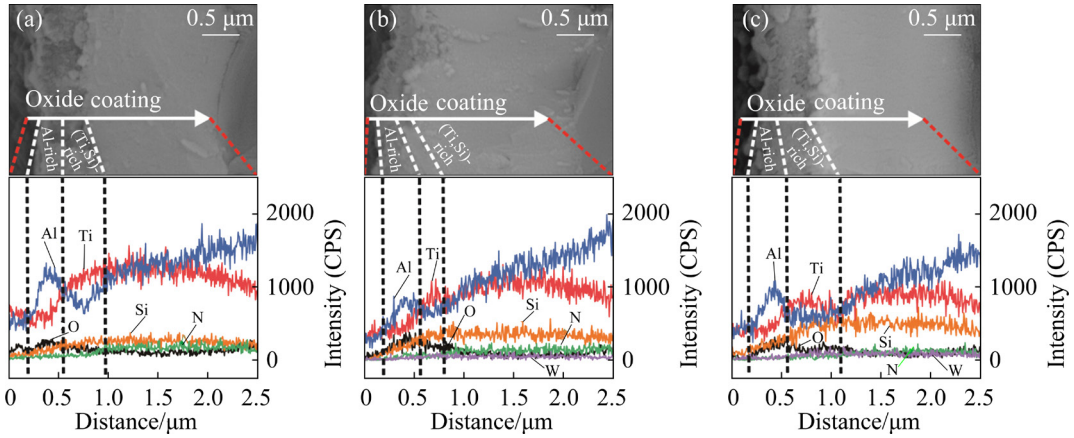

Fig. 7 Fracture cross-sectional SEM images and corresponding EDX line scan profiles of $Ti_{0.46}Al_{0.45}Si_{0.09}N$ (a), $Ti_{0.43}Al_{0.46}Si_{0.08}W_{0.03}N$ (b), and $Ti_{0.41}Al_{0.46}Si_{0.07}W_{0.06}N$ (c) coatings after isothermal oxidation at 1000 °C for 10 h

doping instead leads to the deterioration of the antioxidant properties. As shown in Fig. 6(c), $Ti_{0.41}Al_{0.46}Si_{0.07}W_{0.06}N$ exhibits the highest intensity of *r*-TiO_2 and the lowest intensity of α-Al_2O_3 in the temperature range of 800−1000 °C. Subsequently, $Ti_{0.41}Al_{0.46}Si_{0.07}W_{0.06}N$ experiences a full oxidation at 1100 °C with the oxidation products of *r*-TiO_2, α-Al_2O_3, and $Al_6Si_2O_{13}$.

Cross-sectional SEM images and EDS line scan profiles of $Ti_{0.46}Al_{0.45}Si_{0.09}N$, $Ti_{0.43}Al_{0.46}Si_{0.08}W_{0.03}N$, and $Ti_{0.41}Al_{0.46}Si_{0.07}W_{0.06}N$ coatings on Al_2O_3 substrates after oxidation for 10 h at 1000 °C are shown in Fig. 7. All coatings present a bilayer oxide structure consisting of a dense Al-rich top-layer as well as a porous (Ti,Si)-rich sublayer with thickness of ~0.70 μm for $Ti_{0.46}Al_{0.45}Si_{0.09}N$, ~0.52 μm for $Ti_{0.43}Al_{0.46}Si_{0.08}W_{0.03}N$, and ~0.90 μm for $Ti_{0.41}Al_{0.46}Si_{0.07}W_{0.06}N$, respectively. This is in good accordance with the above results, where the $Ti_{0.43}Al_{0.46}Si_{0.08}W_{0.03}N$ coating obtains the best oxidation resistance.

As for the TiAlN-based coatings, the growth of the Ti-oxide-rich sublayer is usually accompanied by the anatase-to-rutile TiO_2 conversion with an undesired volume shrinkage, which has a detrimental impact on the oxidation resistance [6]. Compared with the $Ti_{0.46}Al_{0.45}Si_{0.09}N$ coating, alloying with 3 at.% W causes the earlier generation of a- and r-TiO_2 during the initial oxidation stage. Nevertheless, the promoted α-Al_2O_3 formation effectively obstructs the inward diffusion of oxygen as well as the outward diffusion of metallic ions, which overcompensates the passive effect of the transformation from metastable a-TiO_2 to stable r-TiO_2. It can be found that the $Ti_{0.43}Al_{0.46}Si_{0.08}W_{0.03}N$ coating shows the thinnest (Ti,Si)-rich sublayer. However, the higher W-addition does not allow early α-Al_2O_3 formation in the $Ti_{0.41}Al_{0.46}Si_{0.07}W_{0.06}N$ coating. Accordingly, the oxidation rate of $Ti_{0.41}Al_{0.46}Si_{0.07}W_{0.06}N$ is much faster than that of $Ti_{0.43}Al_{0.46}Si_{0.08}W_{0.03}N$. Moreover, due to the higher amount of bcc-W phase in the $Ti_{0.41}Al_{0.46}Si_{0.07}W_{0.06}N$ coating, the transformation from the bcc-W toward WO_3 and the subsequent sublimation of WO_3 results in a more severe volume expansion ($V_{\alpha\text{-W}}$=9.95 cm^3/mol and V_{WO_3}=31.83 cm^3/mol), which breaks the Al-rich protective top-layer, leading to a noticeable decline in the oxidation resistance [41−43].

4 Conclusions

(1) Tungsten doping in the coatings forms both substitution solid solution of Ti and/or Al in TiAlN and W simple substance. The $Ti_{0.43}Al_{0.46}Si_{0.08}W_{0.03}N$ and $Ti_{0.41}Al_{0.46}Si_{0.07}W_{0.06}N$ coatings exhibit a mixed c/w-(Ti, Al, Si, W)N and bcc-W three-phase structure. Meanwhile, W-addition optimizes the surface morphology of the TiAlSiN coating.

(2) Incorporation of W into TiAlSiN coating has not obvious effect on the hardness of (29.1±0.4) GPa for $Ti_{0.46}Al_{0.45}Si_{0.09}N$, (29.7±1.1) GPa for $Ti_{0.43}Al_{0.46}Si_{0.08}W_{0.03}N$, and (30.2±1.0) GPa for $Ti_{0.41}Al_{0.46}Si_{0.07}W_{0.06}N$.

(3) Alloying with W into the TiAlSiN coating has a positive effect on thermal stability. The peak hardness values during annealing are (33.9±0.8) GPa for $Ti_{0.43}Al_{0.46}Si_{0.08}W_{0.03}N$ at 1000 °C and

(35.3±1.0) GPa for $Ti_{0.41}Al_{0.46}Si_{0.07}W_{0.06}N$ at 1100 °C, while that of $Ti_{0.46}Al_{0.45}Si_{0.09}N$ is only (33.1±0.8) GPa at 1000 °C.

(4) Moderate W-doping (3 at.%) promotes Al_2O_3 formation and improves the oxidation resistance of TiAlSiN coating. The oxide thicknesses of $Ti_{0.46}Al_{0.45}Si_{0.09}N$, $Ti_{0.43}Al_{0.46}Si_{0.08}W_{0.03}N$, and $Ti_{0.41}Al_{0.46}Si_{0.07}W_{0.06}N$ after oxidation at 1000 °C for 10 h are ~0.70, ~0.52, and ~0.90 μm, respectively.

CRediT authorship contribution statement

Xu SUN: Visualization, Writing − Original draft preparation; **Wen HU:** Investigation; **Li CHEN:** Conceptualization, Methodology, Writing − Review & editing, Funding acquisition; **Jian-chuan WANG:** Writing – Review & editing.

Declaration of competing interest

The authors declare that they have no known competing financial interests or personal relationships that could have appeared to influence the work reported in this paper.

Acknowledgments

This work was financially supported by the National Natural Science Foundation of China (Nos. 51775560, 51771234). LI CHEN and Jian-chuan WANG appreciate the support of the State Key Laboratory of Powder Metallurgy, Central South University, China.

References

[1] HUSSEIN M, KUMAR M, ANKAH N, ABDELAAL A. Surface, mechanical, and in vitro corrosion properties of arc-deposited TiAlN ceramic coating on biomedical Ti6Al4V alloy [J]. Transactions of Nonferrous Metals Society of China, 2023, 33: 494−506.

[2] RACHBAUER R, BLUTMAGER A, HOLEC D, MAYRHOFER P H. Effect of Hf on structure and age hardening of Ti−Al−N thin films [J]. Surface and Coatings Technology, 2012, 206(10): 2667−2672.

[3] TIAN Jin-lian, HU Chun, CHEN Li, LOU Yu-min, ZHAO Ning-ning. Structure, mechanical and thermal properties of Y-doped CrAlN coatings [J]. Transactions of Nonferrous Metals Society of China, 2021, 31(9): 2740−2749.

[4] TAO Xian-cheng, LOU Yu-min, LI Miao-lei, ZHAO Ning-ning, TANG Xiu-zhi, HU Hai-long, HUANG Xiao-zhong, YUE Jian-ling. Microstructure and mechanical properties of VAlN/Si_3N_4 nano-multilayer coatings [J]. Journal of Central South University, 2022, 29(5): 1403−1411.

[5] VEPREK S, JILEK M. Super- and ultrahard nanacomposite coatings: Generic concept for their preparation, properties and industrial applications [J]. Vacuum, 2002, 67(3/4): 443−449.

[6] LIU Zhe-ren, PEI Fei, CHEN Li, MAYRHOFER P H. Effect of Si-addition on structure and thermal stability of Ti−Al−N coatings [J]. Journal of Alloys and Compounds, 2022, 917: 165483.

[7] YU Dong-hai, WANG Cheng-yong, CHENG Xiao-ling, ZHANG Feng-lin. Microstructure and properties of TiAlSiN coatings prepared by hybrid PVD technology [J]. Thin Solid Films, 2009, 517(17): 4950−4955.

[8] MA Quan-sheng, LI Liu-he, XU Ye, MA Xuan, XU Yi, LIU Hong-tao. Effect of Ti content on the microstructure and mechanical properties of TiAlSiN nanocomposite coatings [J]. International Journal of Refractory Metals and Hard Materials, 2016, 59: 114−120.

[9] ZHANG Jie, CHEN Li, KONG Yi, HU Chun, LIU Zhe-ren, DU Yong, ZHANG Shu-yan. Microstructure, mechanical and thermal properties of TiAlTaN/TiAlSiN multilayer [J]. Vacuum, 2021, 187: 110138.

[10] ZHANG Kai, XIN Li, MA Tian-yu, CHANG Hao, LU Yi-liang, FENG Chang-jie, ZHU Sheng-long, WANG Fu-hui. Investigation of the role of silicon in TiAlSiN coating deposited on TiAl alloys during long-term oxidation [J]. Corrosion Science, 2022, 204: 110394.

[11] ZHU Lu, CHEN Peng, CAI Zi-ming, FENG Pei-zhong, KANG Xue-qin, AKHTAR F, WANG Xiao-hong. Fabrication of $MoSi_2$ coatings on molybdenum and its high-temperature anti-oxidation properties [J]. Transactions of Nonferrous Metals Society of China, 2022, 32: 935−946.

[12] PEI Fei, LIU Hui-jun, CHEN Li, XU Yu-xiang, DU Yong. Improved properties of TiAlN coating by combined Si-addition and multilayer architecture [J]. Journal of Alloys and Compounds, 2019, 790: 909−916.

[13] SUN Xu, LIU Zhe-ren, CHEN Li. Influence of Si and Ta mixed doping on the structure, mechanical and thermal properties of Ti−Al−N coatings [J]. Surface and Coatings Technology, 2023, 461: 129428.

[14] AL-RJOUB A, CAVALEIRO A, BIN YAQUB T, EVARISTO M, FIGUEIREDO N M, FERNANDES F. TiAlSiN(Ag) coatings for high temperature applications: The influence of Ag alloying on the morphology, structure, thermal stability and oxidation resistance [J]. Surface and Coatings Technology, 2022, 442: 128087.

[15] ASANUMA H, KLIMASHIN F F, POLCIK P, KOLOZSVARI S, RIEDL H, MAYRHOFER P H. Thermo-mechanical properties and oxidation resistance of Ce−Si alloyed Ti−Al−N thin films [J]. Vacuum, 2019, 166: 231−238.

[16] TIAN Bin, YUE Wen, FU Zhi-qiang, GU Yan-hong, WANG Cheng-biao, LIU Jia-jun. Microstructure and tribological properties of W-implanted PVD TiN coatings on 316L stainless steel [J]. Vacuum, 2014, 99: 68−75.

[17] LIU Dong-guang, ZHENG Liang, LUO Lai-ma, ZAN Xiang, SONG Jiu-peng, XU Qiu, ZHU Xiao-yong, WU Yu-cheng. An overview of oxidation-resistant tungsten alloys for nuclear fusion [J]. Journal of Alloys and Compounds, 2018, 765: 299−312.

[18] SANGIOVANNI D G, CHIRITA V, HULTMAN L.

Toughness enhancement in TiAlN-based quarternary alloys [J]. Thin Solid Films, 2012, 520(11): 4080−4088.

[19] BUCHINGER J, KOUTNÁ N, KIRNBAUER A, HOLEC D, MAYRHOFER P H. Heavy-element-alloying for toughness enhancement of hard nitrides on the example Ti−W−N [J]. Acta Materialia, 2022, 231: 117897.

[20] GLATZ S A, BOLVARDI H, KOLOZSVÁRI S, KOLLER C M, RIEDL H, MAYRHOFER P H. Arc evaporated W-alloyed Ti−Al−N coatings for improved thermal stability, mechanical, and tribological properties [J]. Surface and Coatings Technology, 2017, 332: 275−282.

[21] PSHYK O V, LI X, PETROV I, SANGIOVANNI D G, PALISAITIS J, HULTMAN L, GRECZYNSKI G. Discovery of Guinier−Preston zone hardening in refractory nitride ceramics [J]. Acta Materialia, 2023, 255: 119105.

[22] HU Wen, DU Jian-wei, LIU Zhe-ren, SUN Xu, CHEN Li. Structure, mechanical and thermal properties of TiSiWN coatings [J]. Coatings, 2023, 13(1): 119.

[23] OLIVER W C, PHARR G M. An improved technique for determining hardness and elastic modulus using load and displacement-sensing indentation experiments [J]. Journal of Materials Research, 1992, 7(6): 1564−1583.

[24] HU Chun, CHEN Li, MORAES V. Structure, mechanical properties, thermal stability and oxidation resistance of arc evaporated CrAlBN coatings [J]. Surface and Coatings Technology, 2021, 417: 127191.

[25] PEI Fei, XU Yu-xiang, CHEN Li, DU Yong, ZOU Hou-ke. Structure, mechanical properties and thermal stability of $Ti_{1-x}Si_xN$ coatings [J]. Ceramics International, 2018, 44(13): 15503−15508.

[26] POHLER M, FRANZ R, RAMM J, POLCIK P, MITTERER C. Cathodic arc deposition of $(Al,Cr)_2O_3$: Macroparticles and cathode surface modifications [J]. Surface and Coatings Technology, 2011, 206(6): 1454−1460.

[27] GLATZ S A, KOLLER C M, BOLVARDI H, KOLOZSVÁRI S, RIEDL H, MAYRHOFER P H. Influence of Mo on the structure and the tribomechanical properties of arc evaporated Ti−Al−N [J]. Surface and Coatings Technology, 2017, 311: 330−336.

[28] BARNA P B, ADAMIK M. Fundamental structure forming phenomena of polycrystalline films and the structure zone models [J]. Thin Solid Films, 1998, 317(1/2): 27−33.

[29] VEPREK S, ZHANG R F, VEPREK-HEIJMAN M G J, SHENG S H, ARGON A S. Superhard nanocomposites: Origin of hardness enhancement, properties and applications [J]. Surface and Coatings Technology, 2010, 204(12/13): 1898−1906.

[30] MCINTYRE D, GREENE J E, HÅKANSSON G, SUNDGREN J E, MÜNZ W D. Oxidation of metastable single–phase polycrystalline $Ti_{0.5}Al_{0.5}N$ films: Kinetics and mechanisms [J]. Journal of Applied Physics, 1990, 67(3): 1542−1553.

[31] DU Jian-wei, CHEN Li, ZHANG Jie, XU Yu-xiang, LIU Zhe-ren, PEI Fei. Tuning mechanical properties of TiAlSiN/TiAlN multilayers by interfacial structure [J]. Materials Characterization, 2024, 210: 113836.

[32] WILLMANN H, MAYRHOFER P H, PERSSON P O Å, REITER A E, HULTMAN L, MITTERER C. Thermal stability of Al−Cr−N hard coatings [J]. Scripta Materialia, 2006, 54(11): 1847−1851.

[33] WANG Hui-ting, XU Yu-xiang, CHEN Li. Optimization of Cr−Al−N coating by multilayer architecture with TiSiN insertion layer [J]. Journal of Alloys and Compounds, 2017, 728: 952−958.

[34] RACHBAUER R, GENGLER J J, VOEVODIN A A, RESCH K, MAYRHOFER P H. Temperature driven evolution of thermal, electrical, and optical properties of Ti−Al−N coatings [J]. Acta Materialia, 2012, 60(5): 2091−2096.

[35] MORENO M, ANDERSSON J M, JOHANSSON-JÖESAAR M P, FRIEDRICH B E, BOYD R, SCHRAMM I C, JOHNSON L J S, ODÉN M, ROGSTRÖM L. Wear of Mo- and W-alloyed TiAlN coatings during high-speed turning of stainless steel [J]. Surface and Coatings Technology, 2022, 446: 128786.

[36] SALAMANIA J, FARHADIZADEH A F, CALAMBA KWICK K M, SCHRAMM I C, HSU T W, JOHNSON L J S, ROGSTRÖM L, ODÉN M. Influence of nitrogen vacancies on the decomposition route and age hardening of wurtzite $Ti_{1-x}Al_xN_y$ thin films [J]. Journal of Vacuum Science & Technology A, 2023, 41(6): 063413.

[37] TASNÁDI F, ABRIKOSOV I A, ROGSTRÖM L, ALMER J, JOHANSSON M P, ODÉN M. Significant elastic anisotropy in $Ti_{1-x}Al_xN$ alloys [J]. Applied Physics Letters, 2010, 97: 231902.

[38] KRZANOWSKI J E. The effect of composition profile shape on the strength of metallic multilayer structures [J]. Scripta Metallurgica et Materialia, 1991, 25(6): 1465−1470.

[39] WU Guo-long, ZHANG Shuo, WANG Ye, SUN Min, ZHANG Qun-li, KOVALENKO V, YAO Jian-hua. Porous ceramic coating formed on 316L by laser cladding combined plasma electrolytic oxidation for biomedical application [J]. Transactions of Nonferrous Metals Society of China, 2022, 32(9): 2993−3004.

[40] TIAN Yu-xin, XIAO Hua-qiang, YOU Chuan-chuan, FENG Jin-yu, XIAO Yi, ZHOU Xuan. High-temperature oxidation and wear properties of laser cladded Ti−Al−N composite coatings [J]. Transactions of Nonferrous Metals Society of China, 2023, 33(6): 1779−1791.

[41] JAVDOŠŇÁK D, MUSIL J, SOUKUP Z, HAVIAR S, ČERSTVÝ R, HOUSKA J. Tribological properties and oxidation resistance of tungsten and tungsten nitride films at temperatures up to 500 °C [J]. Tribology International, 2019, 132: 211−220.

[42] LIU Yu-heng, CHANG Li-chun, LIU Bo-wei, CHEN Yung-i. Mechanical properties and oxidation behavior of W−Si−N coatings [J]. Surface and Coatings Technology, 2019, 375: 727−738.

[43] MACÍAS H A, YATE L, COY L E, APERADOR W, OLAYA J J. Influence of Si-addition on wear and oxidation resistance of $TiWSi_xN$ thin films [J]. Ceramics International, 2019, 45(14): 17363−17375.

W 掺杂对 TiAlSiN 涂层显微组织、力学及热性能的影响

孙 旭[1]，胡 文[2]，陈 利[1,2]，王建川[1]

1. 中南大学 粉末冶金国家重点实验室，长沙 410083；
2. 株洲钻石切削刀具股份有限公司，株洲 412007

摘 要：通过扫描电子显微镜、X 射线衍射仪、差示扫描量热仪和纳米压痕仪等设备研究 W 掺杂对 TiAlSiN 涂层结构和性能的影响。W 在 TiAlSiWN 涂层中以固溶和单质 W 的形式混合存在。添加 W 改善了 TiAlSiN 涂层的表面质量。沉积态 $Ti_{0.46}Al_{0.45}Si_{0.09}N$、$Ti_{0.43}Al_{0.46}Si_{0.08}W_{0.03}N$ 和 $Ti_{0.41}Al_{0.46}Si_{0.07}W_{0.06}N$ 涂层的硬度分别为(29.1±0.4)、(29.7±1.1)和(30.2±1.0) GPa。在退火过程中，$Ti_{0.41}Al_{0.46}Si_{0.07}W_{0.06}N$ 涂层在 1100 ℃时的峰值硬度为(35.3±1.0) GPa，而 $Ti_{0.46}Al_{0.45}Si_{0.09}N$ 和 $Ti_{0.43}Al_{0.46}Si_{0.08}W_{0.03}N$ 涂层在 1000 ℃时的峰值硬度仅为(33.1±0.8)和(33.9±0.8) GPa。此外，适量的 W 掺杂(3 at.%)有利于改善 TiAlSiN 涂层的抗氧化性。$Ti_{0.46}Al_{0.45}Si_{0.09}N$ 和 $Ti_{0.41}Al_{0.46}Si_{0.07}W_{0.06}N$ 涂层在 1000 ℃下氧化 10 h 后的氧化层厚度分别为~0.70 和~0.90 μm，然而 $Ti_{0.43}Al_{0.46}Si_{0.08}W_{0.03}N$ 涂层的氧化层厚度仅为~0.52 μm。

关键词：TiAlSiWN 涂层；阴极弧蒸发；结构演变；硬度；热稳定性；抗氧化性

(Edited by Xiang-qun LI)